17th International Conference on the Application of Computer
Science and Mathematics in Architecture and Civil Engineering
K. Gürlebeck and C. Könke (eds.)
Weimar, Germany, 12–14 July 2006

DISCRETE CRACK SIMULATION OF CONCRETE USING THE EXTENDED FINITE ELEMENT METHOD

J.F. Unger* **and C. Könke**

**Institute of Structural Mechanics, Bauhaus-University Weimar,*
Marienstraße 15, 99423 Weimar, Germany
E-mail: joerg.unger@bauing.uni-weimar.de

Keywords: Extended Finite Element Method, cohesive crack, concrete

Abstract. *The extended finite element method (XFEM) offers an elegant tool to model material discontinuities and cracks within a regular mesh, so that the element edges do not necessarily coincide with the discontinuities. This allows the modelling of propagating cracks without the requirement to adapt the mesh incrementally. Using a regular mesh offers the advantage, that simple refinement strategies based on the quadtree data structure can be used to refine the mesh in regions, that require a high mesh density. An additional benefit of the XFEM is, that the transmission of cohesive forces through a crack can be modelled in a straightforward way without introducing additional interface elements. Finally different criteria for the determination of the crack propagation angle are investigated and applied to numerical tests of cracked concrete specimens, which are compared with experimental results.*

1 INTRODUCTION

The extended finite element method (XFEM) is often used to model cracks and crack growth, since a crack can be described independently of the background mesh [1]. That allows the usage of regular meshes, which facilitates the mesh generation. Another interesting feature of the XFEM is, that material discontinuities can be represented without the requirement, that element edges coincide with the material discontinuity [2].

Cracking in concrete is characterized by coalescence of microcracks, which finally join to a macroscopic discrete crack. This phenomenon can be modeled using the cohesive zone approach, where stresses can be transferred through the interface accounting for the process zone. An important point for automatic crack growth simulations is the criteria, that determines the orientation and position of a new a crack, and how the crack propagation direction is determined. In this paper different methods are compared to verify the applicability of each method.

2 EXTENDED FINITE ELEMENT METHOD

The Extended finite element method [1] offers the possibility to model cracks and interfaces between different materials independently of the mesh. The general idea is to enrich the displacement interpolation with special purpose functions

$$\mathbf{d}(\mathbf{x}) = \sum_{i=1}^{N_{tot}} \phi_{i,std}(\mathbf{x}) d_{i,std} + \sum_{j=0}^{N_{enr}} \Psi(\mathbf{x}) \phi_{j,enr}(\mathbf{x}) d_{j,enr}, \tag{1}$$

where N_{tot} is the total number of nodes and N_{enr} the number of enriched nodes. $\phi_{i,std}$ are the standard shape functions, whereas the enriched interpolation is a product of the shape functions $\phi_{j,enr}$, which fullfil the partition of unity, and the enrichment functions $\Psi(\mathbf{x})$. $d_{i,std}$ and $d_{j,enr}$ are the standard and enriched nodal displacements. The interpolation in Equation 1 is used in a standard Galerkin method:

$$\mathbf{Kd} = \mathbf{f} \qquad \text{with} \tag{2}$$

$$\mathbf{K}_{IJ} = \int_{\Omega} \mathbf{B_I}^T \mathbf{C} \mathbf{B_J} \tag{3}$$

$$\mathbf{f}_I = \int_{\Gamma^t} \phi_I \mathbf{t}, \tag{4}$$

where $\mathbf{B}_i$ contains the derivatives of the shape/enrichment functions and $\mathbf{C}$ is the material matrix for a linear elastic material and $\mathbf{t}$ are prescribed tractions on the boundary.

2.1 Cracks

Cracks are characterized by a discontinuous displacement field and as a result the Heaviside function

$$H(\mathbf{x}) = \left\{ \begin{array}{cc} -1 & \mathbf{x} \epsilon \Omega_- \\ 1 & \mathbf{x} \epsilon \Omega_+ \end{array} \right\}, \tag{5}$$

can be used as a special purpose function $\Psi(\boldsymbol{x})$, where Ω_-, Ω_+ are the negative and positive sides of the crack and $\mathbf{x}$ is a vector with the coordinates (x_1, x_2). Using only the Heaviside function as an enrichment function requires the cracktips to be on element edges. A more elegant way is to use crack tip functions, which further enables the interpolation to represent

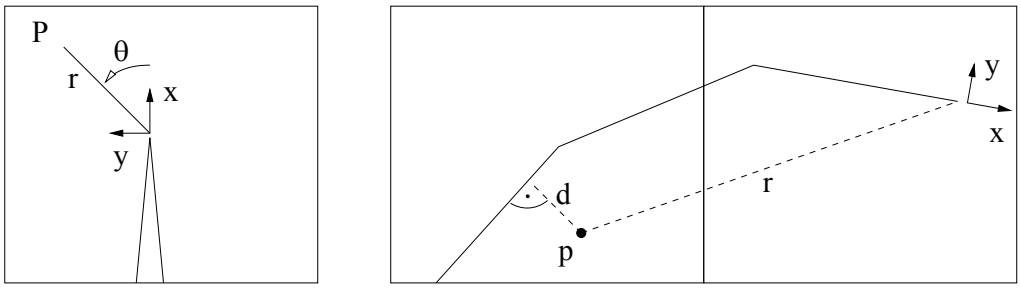

Figure 1: crack tip coordinate system and transformation for curved cracks

singular stress fields as assumed in linear elastic fracture mechanics. For stress free cracks the following functions are used as special pupose function Ψ:

$$\Psi_{\alpha,LEFM,\alpha=1..4} = \sqrt{r}\left[\sin\left(\frac{\theta}{2}\right), \cos\left(\frac{\theta}{2}\right), \sin(\theta)\sin\left(\frac{\theta}{2}\right), \sin(\theta)\cos\left(\frac{\theta}{2}\right)\right]. \quad (6)$$

2.2 Transformation for curved cracks

The crack tip functions given in Equation 6 represent the theoretical near tip displacement field for straight cracks. For curved cracks a modification has to be performed, to ensure, that the discontinuity remains on the crack. Different possibilities are presented in [3, 4]. In our paper a transformation is used, that results in a continuous displacement field on each side of the crack trajectory. The angle θ is modified (see Figure 1)

$$\theta = \arcsin\left(\frac{d}{r}\right). \quad (7)$$

For strongly curved cracks the interpolated displacement field can not be represented accurately and a mesh refinement is required.

2.3 Cohesive Cracks

Within the framework of the Extended Finite Element Method the incorporation of cohesive cracks is straightforward [5]. If a cohesive crack is present, the internal energy has to be modified to account for the additional cohesive forces, transfered through the crack:

$$\Pi_i = \frac{1}{2}\int_\Omega \boldsymbol{\sigma}^T\boldsymbol{\varepsilon}\, d\Omega + \int_{\Gamma_{coh}} \boldsymbol{t}^T\boldsymbol{u}\, \boldsymbol{d}\Gamma_{coh} \quad (8)$$

$$\delta\Pi_i = \left[\int_\Omega \boldsymbol{B}^T\boldsymbol{C}\boldsymbol{B}\, d\Omega + \int_{\Gamma_{coh}} \bar{\boldsymbol{B}}^T\bar{\boldsymbol{C}}\bar{\boldsymbol{B}}\, d\Gamma_{coh}\right]\boldsymbol{d}, \quad (9)$$

where $\boldsymbol{t}$ is the force per area transferred through the crack, $\boldsymbol{u}$ the opening displacement of the crack and Γ_{coh} the cracksurface. The crack opening is a function of the nodal displacements $\boldsymbol{d}$ and the difference between the corresponding shape functions on the negative and positive side of the crack, arranged in the matrix $\bar{\boldsymbol{B}}$:

$$\boldsymbol{u} = \bar{\boldsymbol{B}}\boldsymbol{d}. \quad (10)$$

Furthermore the forces transferred through the crack are a function of the crack opening

$$\boldsymbol{t} = \bar{\boldsymbol{C}}\boldsymbol{u}, \quad (11)$$

with $\bar{C}$ the interface material matrix. In this paper the modified version of the nonlinear interface model [6] has been used, which is explained in section 5.
An important point in the numerical application is the integration of the system matrices along Γ_{coh} of the cohesive cracks in Equation 8. Since the applied interface law has a softening part, a Gauss-point quadrature leads to numerical instabilities. The extrapolation from the integration points within the element to the extreme values at the end of a crack segment will result in many cases in an overestimation of the stiffness. In order to circumvent this problem, a Newton-Cotes integration has been applied, and a better convergence behaviour of the numerical solution could be observed.
If a cohesive model is applied, the assumption of a singular stress field at the crack tip is no longer fulfilled. In [5] the following enrichment functions for the cohesive crack tip are proposed, which are used in the following:

$$\Psi_{\alpha,coh,\alpha=1..4} = r\left[\sin\left(\frac{\theta}{2}\right), \cos\left(\frac{\theta}{2}\right), \sin(\theta)\sin\left(\frac{\theta}{2}\right), \sin(\theta)\cos\left(\frac{\theta}{2}\right)\right]. \qquad (12)$$

3 REFINEMENT USING THE QUADTREE DATA STRUCTURE

As described in the previous section, the X-FEM offers an efficient tool to model cracks without the requirement, that the element edges coincide with the discontinuity. Starting with an initial coarse mesh, an efficient refinement strategy is required, that increases the node density in regions, where a higher node density is required, e.g. close to a crack tip or in the vicinity of material discontinuities.
This can be achieved by using the Quadtree data structure (and for 3D applications the Octree data structure), for which a good overview can be found in [7]. Starting with an initial mesh, the elements are iteratively decomposed into 4 subelements until the required accuracy is reached. The shape of the initial elements determines the shape of their subelements, so a square is decomposed into a 4 squares and a rectangle into 4 rectangles. Using this approach any polygonal bounded domain can be refined, if an initial mesh can be created. If two neighboring elements are not on the same refinement level, additional effort is required. [8] proposed a mapping of regular elements with 5 to 7 nodes, that are positioned (equally spaced) on the unit circle. Within these elements the natural neighbor interpolation is used, which is linear between nodes on the boundary and as a result the coupling with linear finite elements is compatible. This procedure gives accurate results, although the interpolant is not a polynomial and as a result the Gauss quadrature for the integration of the stiffness matrix is only an approximation. A second possibility, applied in this paper, is to set up additional constrained equations, that couple the ”hanging nodes” with the nodes of the adjacent coarser element. It is further recommended to limit the difference in the refinement level between two neighboring elements to one in order to obtain a smooth variation of the node density within the domain. By applying this quadtree structure the number of degrees of freedom of the structure can be considerably reduced without loss of accuracy, compared to a regular mesh refinement preformed for the complete mesh.

An example for the subdivision of an ellipse is illustrated in Figure 2.

4 CRACK INITIATION AND CRACK EXTENSION

In order to initiate a crack the principal stresses at all integration points are examined. If the principal stress exceeds the tensile strength of the material, a new crack is introduced, or-

thogonal to the corresponding eigenvector with a prescribed length in both directions from the integration point.

The decision, whether an existing crack progagates is based on the energy release rate, which is calculated from the virtual crack extension technique [9].

$$G = \frac{\partial \Pi}{\partial a} = \frac{\partial (U_p + E_s)}{\partial a} = \frac{\partial (W_f - U_{el})}{\partial a} \tag{13}$$

with G is the energy release rate, W_f the work performed by the external forces, U_{el} and U_{pl} the elastic and plastic internal strain energy, E_s the surface energy and a the crack length. Under displacement control the work performed by the external forces due to a crack elongation vanishes and as a result can be neglected. Finite differences with a short increment δa are used to approximate the derivative with respect to a.

$$G = \frac{U_p(a + \delta a) + E_s(a + \delta a) - U_p(a) - E_s(a)}{\delta a} \tag{14}$$

Only the energy of the crack tip element and its neighbors has to be considered in Equation 14, since the displacements and as a result the strain energy within the other elements is not influenced by a virtual crack extension.

Three different approaches have been investigated to determine the direction of the crack extension. The first one is a nonlocal criterium, which evaluates a nonlocal stress within the prescribed radius in the vicinity of the crack tip. The direction is then determined orthogonal to the eigenvector of the second principal stress. This criterion lead to oscillating crack directions, especially due to the fact, that the stresses within the vicinity of the crack are not correctly approximated with the XFEM. An additional problem occurs for crack tips, that are close to domains in compression.

The second criterion is the displacement correlation technique based on the assumptions of LEFM. Assuming a stress free crack, the near tip displacements around the tip in a polar crack tip coordinate system are given by

$$\begin{aligned} u_1 = \quad & K_1 \tfrac{1}{2\mu} \sqrt{\tfrac{r}{2\pi}} \cos\left(\tfrac{\theta}{2}\right) \left(\kappa - 1 + 2\sin^2\left(\tfrac{\theta}{2}\right)\right) \\ & + K_2 \tfrac{1}{2\mu} \sqrt{\tfrac{r}{2\pi}} \sin\left(\tfrac{\theta}{2}\right) \left(\kappa + 1 + 2\cos^2\left(\tfrac{\theta}{2}\right)\right) \end{aligned} \tag{15}$$

$$\begin{aligned} u_2 = \quad & K_1 \tfrac{1}{2\mu} \sqrt{\tfrac{r}{2\pi}} \sin\left(\tfrac{\theta}{2}\right) \left(\kappa + 1 - 2\cos^2\left(\tfrac{\theta}{2}\right)\right) \\ & - K_2 \tfrac{1}{2\mu} \sqrt{\tfrac{r}{2\pi}} \cos\left(\tfrac{\theta}{2}\right) \left(\kappa - 1 - 2\sin^2\left(\tfrac{\theta}{2}\right)\right) \end{aligned} \tag{16}$$

with $\kappa = \frac{3-\nu}{1+\nu}$ for plane stress, $\kappa = 3 - 4\nu$ for plane strain and $\mu = \frac{E}{2(1+\nu)}$. The crack opening is calculated for certain positions close to the crack tip, where the cohesive forces of the crack

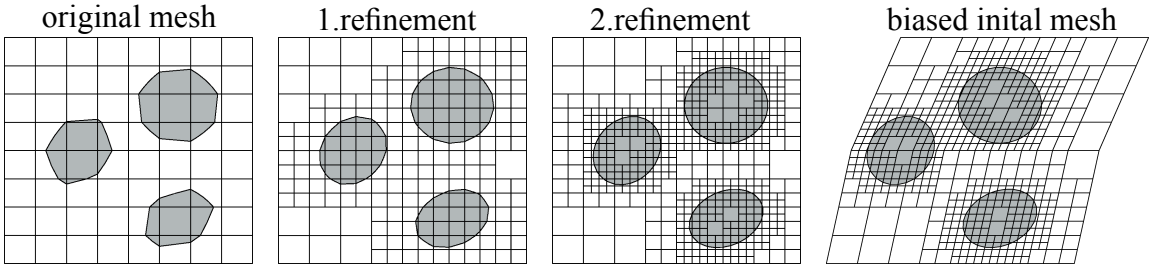

Figure 2: adaptation of a mesh using the quadtree data structure

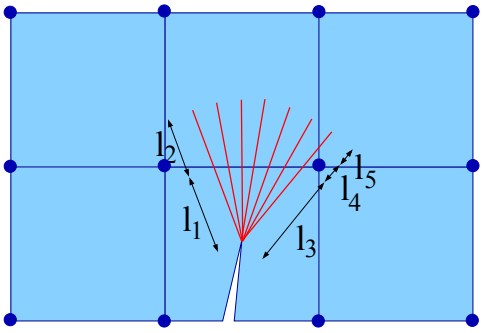

Figure 3: extension of the crack in different directions

to be extended are neglected. This implies the assumption, that cohesive and stress free cracks grow in the same direction. By using the calculated crack opening displacements near the tip and substituting them into Equations (15,16) virtual stress intensity factors can be calculated. The maximum circumferential tensile stress criterion finally gives the direction of the crack extension:

$$\tan\left(\frac{\theta}{2}\right) = \frac{1}{4}\frac{K_I}{K_{II}} \pm \frac{1}{4}\sqrt{\left(\frac{K_I}{K_{II}}\right)^2 + 8} \tag{17}$$

The third criterion for the crack extension is an energy based criterion. It is assumed, that the crack with a prescribed crack extension grows in the direction, that minimizes the potential energy of the system.

$$\Pi = W_f - U_{el} \rightarrow min \tag{18}$$

For several crack extension angles the potential energy of the system is calculated. An equidistant subdivision of the crack extension angle ϕ varying from $[-\phi_{max}, \phi_{max}]$ is used. This is illustrated in Figure 3. From the obtained data a Moving Least Squares (MLS) approximation of the energy as a function of the crack extension angle is performed. A problem of this method arises from the fact, that for different extension angles the length of the segment of the crack extension within an element is different. In Figure 3 the first crack extension is divided into segments with length $l_1 + l_2$ whereas the last extension is divided into segments with length $l_3 + l_4 + l_5$. If a cohesive crack is loaded, the integration points on the segments of a crack reach the tensile strength and pass into the softening part. In general all the integration points within one segment are in the same state (penalty stiffness until peak, softening afterwards). The load displacement curve for such a cohesive crack depends on the number of segments. In the limit case of one segment a sudden crack opening is obtained, when all the integration points on that segment reach the tensile strength. The other limit case is an inifite number of subdivisions. Here the segments pass one after another from the penalty part to the softening regime starting from the segments away from the crack tip, which leads to a smooth curve. The same effect is obtained for the different crack extension angles. If the integration points on a crack segment do not pass the tensile strength, almost no energy is dissipated. In order to make the proposed method objective, it has to be assured, that almost all of the segments open (the integration points are in the softening regime). In order to avoid performing this test after all the different directions have been calculated, in a first step the straight crack extension is tested. The applied load/displacement is increased until all the segments of the crack extension are within the softening regime. Using this load/displacement the test for the different directions is performed.

5 INTERFACE MODEL

A cohesive zone model, that describes normal as well as tangential tractions along an interface, is used. The model is based on [6]. A total crack opening λ is introduced:

$$\lambda = \sqrt{u_n^2 + (\alpha u_t)^2}, \tag{19}$$

where u_n and u_t are the normal and tangential crack opening displacement of the interface, and α is a material constant, that controls the weighting between the normal and tangential opening. Furthermore a cohesive traction-separation law is used:

$$\sigma(\lambda) = \left\{ \begin{array}{cc} K_p\lambda & \lambda < \lambda_0 \\ f_{ct}e^{\frac{-f_{ct}(\lambda-\lambda_0)}{G_f}} & \text{otherwise} \end{array} \right\} \tag{20}$$

with $\lambda_0 = f_{ct}/K_p$ is the crackopening, at which the linear elastic peak load is reached, K_p the penalty stiffness, f_{ct} the thensile strength of the interface layer and G_f its fracture energy.

Assuming, that there exist a potential Φ

$$\Phi(u_n, u_t) = \int_0^\lambda \sigma(\lambda')d\lambda' \tag{21}$$

the normal and tangential tractions are obtained respectively by:

$$T_n = \frac{\partial\Phi(u_n, u_t)}{\partial u_n} = \sigma(\lambda)\frac{u_n}{\lambda} \tag{22}$$

$$T_t = \frac{\partial\Phi(u_n, u_t)}{\partial u_t} = \sigma(\lambda)\frac{\alpha^2 u_t}{\lambda}. \tag{23}$$

Describing the total potential as a function of the mixed displacement leads to the assumption, that the fracture energy in mode I and mode II direction is equivalent, which differs from the general assumption, that mode II fracture energy for concrete is higher than for mde I. Furthermore the obtained stiffness matrix is symmetric. The model requires 4 input parameters, namely the fracture energy G_f, the tensile strength f_{ct}, the parameter α and the penalty stiffness K_p, which has to be chosen carefully. On the one hand the penetration of the two sides of the interface in compression has to be reduced, but on the other hand a high penalty stiffness results in an ill-conditioned stiffness matrix. In the model proposed by [6] an additional parameter (the fracture energies in mode I and mode II are not identical) is required, but the symmetry of the stiffness matrix is lost.

The expression in Equations (22,23) applies for $\dot{\lambda} \geq 0$ and $\lambda = \lambda_{max}$. Otherwise an elastic unloading to the origin is assumed:

$$T_n = \sigma(\lambda_{max})\frac{u_n}{\lambda_{max}} \tag{24}$$

$$T_t = \sigma(\lambda_{max})\frac{\alpha^2 u_t}{\lambda_{max}}. \tag{25}$$

If the interface is in compression, the contact condition is approximated by a penalty stiffness

$$T_n = K_p u_n \tag{26}$$

and the parameter λ is only a function of the tangential displacement.

$$\lambda = |\alpha u_t|. \tag{27}$$

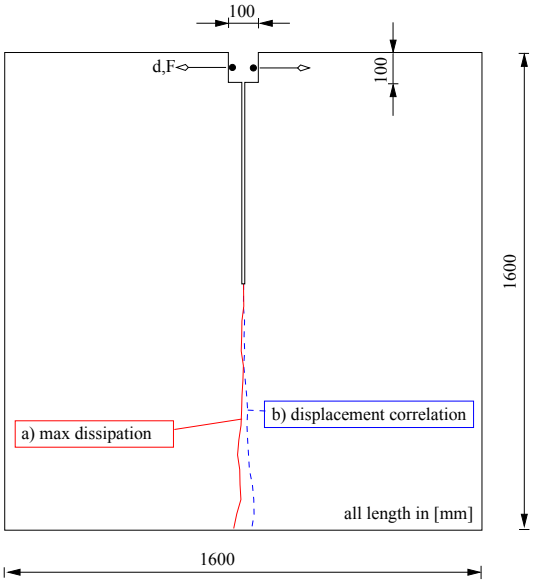

Figure 4: crack path using different criterias for the crack extension a)maximum dissipated energy b) displacement correlation

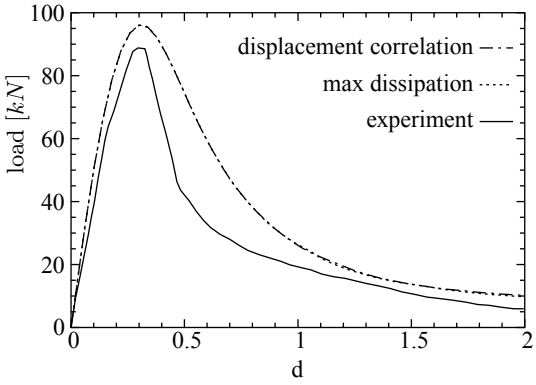

Figure 5: load-displacement curve for the wedge-splitting test with displacement correlation and maximum dissipated energy as direction criterion for the crack extension (almost identical) compared to experimental results

6 EXAMPLES

6.1 Wedge-splitting

In the first example a wedge splitting test is investigated [10]. The geometry of the test specimen is illustrated in Figure 4 with a thickness of 400mm. Young's modulus, Poisson ratio, uniaxial tensile strength and specific fracture energy are given as $E = 28300\ N/mm^2$, $\nu = 0.18$, $f_{ct} = 2.11\ N/mm^2$, $G_f = 0.482\ Nmm/mm^2$. In addition the penalty stiffness for the interface material law $K_p = 25\ 10^4 N/mm^3$ and $\alpha = 1$. In this mode I dominated example the choice of α has only a marginal influence on the result. The model consists of triangular elements with 6 nodes, but only the corner nodes are enriched with special purpose functions. Different criteria for the direction of a crack extension are compared. As can be verified in Figure 5, the obtained load-displacement curves show a good correspondance with the experimental data. Although the crack path slightly varies (see Figure 4), the load-displacement curve is almost identical for both numerical models. The deviation from the theoretically straight vertical crack path is due to unsymmetries caused by the unsymmetric triangular mesh. A second source of error for the maximum energy dissipation criteria is the problem of partly closed crack extensions, which is in detail discussed in 4.

6.2 L-panel

In a second example a mixed mode problem is investigated. The experimental crack path is curved and the correct determination of the crack path with the two presented approaches (displacement correlation and maximum dissipated energy) is investigated. Furthermore the influence of the shear component on the load-displacement curve and the crack direction is investigated. The L-panel test has been performed by [10]. The geometry of the test specimen is illustrated in Figure 6 and its thickness is $t = 100\ mm$. A vertical displacement d is applied on the lower horizontal surface of the horizontal leg at a distance of 30 mm from the vertical end face and the resulting vertical force is measured. The scatter of the obtained crack paths for different experiments is plotted in Figure 6. Young's modulus, Possion ratio, uniaxial tensile strength and the specific fracture energy are given as $E = 25850N/mm^2$, $\nu = 0.18$, $f_{ct} = 2.70N/mm^2$ and $G_f = 0.09Nmm/mm^2$. In order to match the initial elastic part of the load

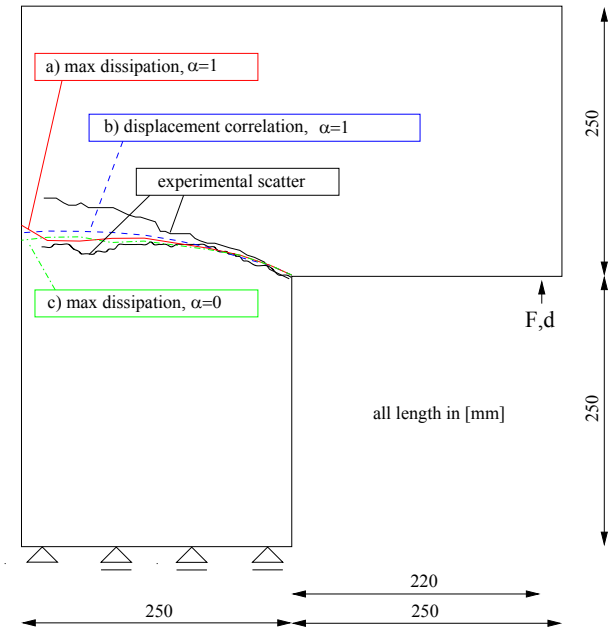

Figure 6: crack path using different criterias for the crack extension and different material properties for the interface a)maximum dissipated energy and $\alpha = 1$ b)displacment correlation and $\alpha = 1$ c)maximum dissipated energy and $\alpha = 0$

displacement curve, the peak load and the softening part, the Young's modulus was modified to $E = 20000N/mm^2$, the tensile strength $f_{ct} = 2.50N/mm^2$ and the specific fracture energy $G_f = 0.13Nmm/mm^2$. The applied mesh is given in Figure 7. An example of the obtained discretization is illustrated in Figure 7 at the beginning with 1529 DOFs (degrees of freedom) and at the end of the calculation with 2643 DOFs. Quadrilateral elements with 9 nodes have been used, but only the corner nodes are enriched with additional special purpose functions. The maximum tensile stress in the elastic part of the loading is obtained at an integration point close to the theoretical location of the stress singularity in the corner. As a result the initial crack starts not exactly at the corner. For the interpretation of the experimental results the origins of the numerically obtained crack paths were moved to the inner corner of the L-panel. The load-displacement curves (measured material data and adapted data) is illustrated in Figure 8. The numerical curves were obtained using the displacement correlation technique and $\alpha = 1$, but there was no significant difference between the load-displacement curves using $\alpha = 0$

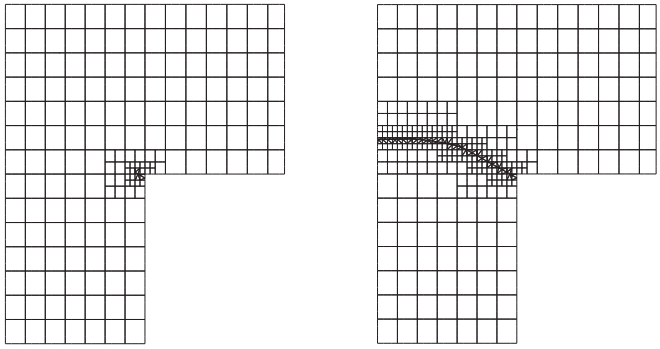

Figure 7: regular quadrilateral element mesh obtained by using an adaptive quadtree refinement algorithm at the beginning and at the end of the calculation (triangular integration zones are plotted in elements enriched by the crack

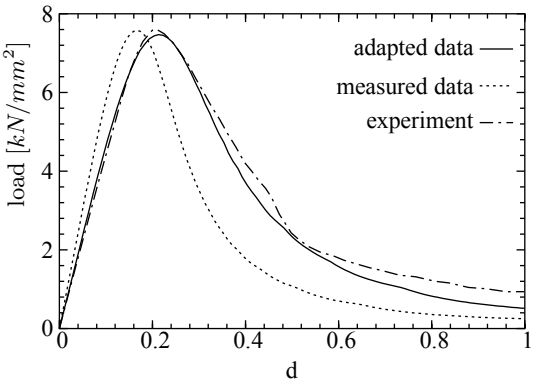

Figure 8: load-displacement curve for the L-panel test with displacement correlation, $\alpha = 1$ and quadrilaterial elements

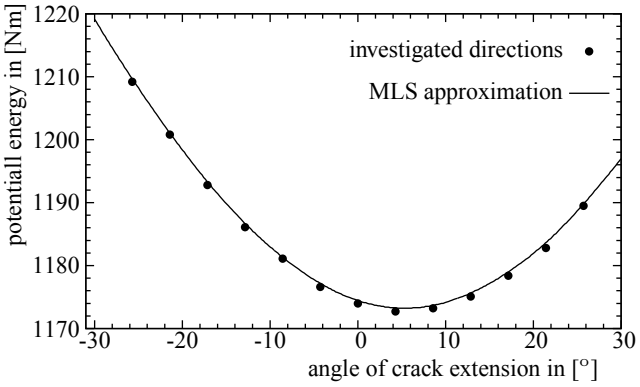

Figure 9: Potential energy of the system for different angles of crack extension

or the maximum dissipated energy criterion. It is to be noted, that $\alpha = 0$ corresponds to the standard cohesive crack model without tangential stresses. A difference was obtained for the crack path, although all models are in the range of the experimental scatter (see Figure 6). A total of 15 directions within the range [-30^o,30^o] were tested for the maximum energy dissipation criterion. The potential energy for different extensions angles for the first crack increment is plotted in Figure 9. The minimum of the potential energy is clearly visible at 5, which leads to a kinking of the crack. For this example the displacement correlation technique is more efficient to calculate the angle of crack propagation, since the total number of nonlinear solution steps for each possible direction is computationally more demanding without giving significantly better results.

6.3 Mixed mode fracture test

The last example is a mixed-mode fracture test performed by [11]. In this paper only the fracture tests 4a and 4b are considered (specimen 48-03 and 46-05). The dimensions are 200x200x50mm with a notch depth of 25mm and a notch width of 5mm as illustrated in Figure 10. The compressive strength from cubes with dimension 150mm and the splitting tensile strength are given as $f_c = 46.24\,N/mm^2$, $f_s = 3.67\,N/mm^2$ for specimen 4a and $f_c = 49.66\,N/mm^2$, $f_s = 3.76\,N/mm^2$ for specimen 4b. The Young's modulus, Poisson ratio and fracture energy were not measured and similar to [12] they were chosen as

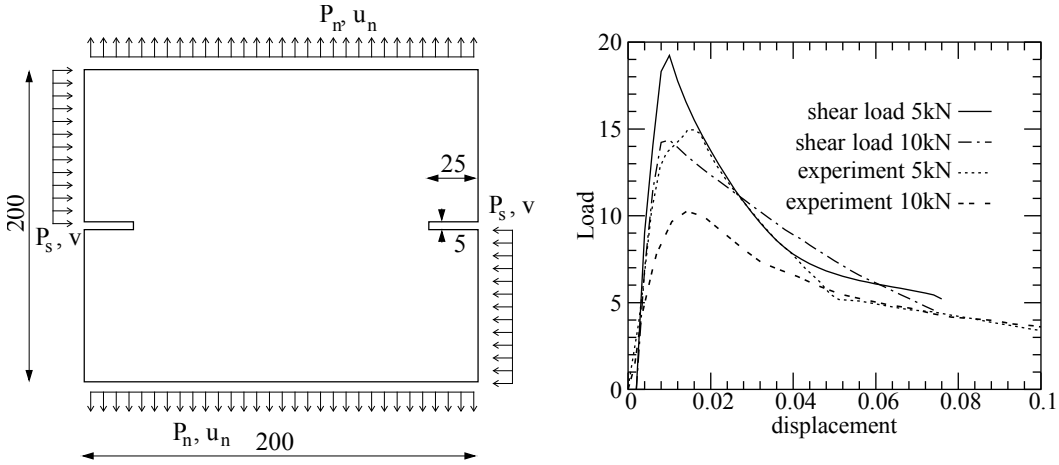

Figure 10: geometry of the specimen for the mixed mode fracture test and load-displacement curve

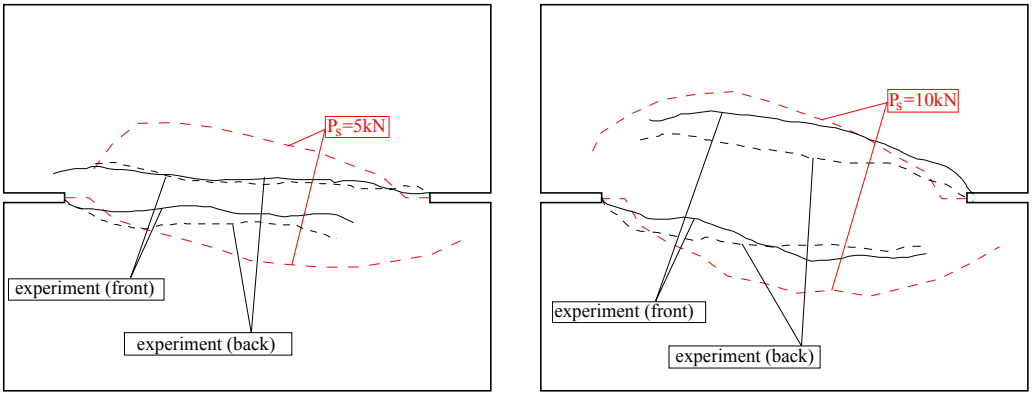

Figure 11: crack path for mixed mode fracture test 4a(left) and 4b(right)

$E = 30000\,N/mm^2$, $\nu = 0.2$ and $G_f = 0.110\,Nmm/mm^2$. The unaxial tensile strength was estimated from the splitting tensile strength as $f_{ct} = 3.0\,N/mm^2$.
A shear force $\mathrm{P_s}$ was applied under displacement control up to 5kN for series 4a and 10kN for series 4b. Afterwards the shear load was kept constant and the specimen was loaded in normal direction $\mathrm{P_n}$ under displacement control. The obtained experimental load-displacement curves are given in Figure 10. In this example the direction of crack extension was determined with the displacement correlation technique. In Figure 11 the obtained crack paths for specimens 4a and 4b are compared with the experimental results. In general the curved crack can be reproduced in the numerical simulation, although for specimen 4a with a relative low shear load the crack curvature obtained from the numerical simulation is overestimated compared to the experiment.

7 CONCLUSIONS

In this paper the applicability of the XFEM for the simulation of concrete structures has been investigated. Cohesive cracks can be modeled within the presented approach without the requirement, that material edges and cracks coincide with finite element edges. The general shape of the load-displacement curve could be accurately represented. The determination of the crack extension angle using the minimum of the potential energy gives accurate predictions for the extension angle, but requires additional computations. Especially if many cracks are present within a structure, the assumption, that a cohesive crack and a stress free crack grow in the same direction is much more efficient. The quadtree data structure can be used to adaptively increase the accuracy close to the moving crack tip, and as a result the numerical effort can be reduced considerably compared to regular mesh refinement in the whole domain.

REFERENCES

[1] N. Moës, J. Dolbow, and T. Belytschko. A finite element method for crack growth without remeshing. *International Journal for Numerical Methods in Engineering*, 46(1):131–150, 1999.

[2] N. Sukumar, D.L. Chopp, N. Moës, and T. Belytschko. Modelling holes and inclusions by level sets in the extended finite-element method. *Computation Methods in applied mechanics and engineering*, 190:6183–6200, 2001.

[3] T. Belytschko and T. Black. Elastic crack growth in finite elements with minimal remeshing. *International journal for numerical methods in engineering*, 45(5):6001–6020, 1999.

[4] T. Belytschko, N. Moës, S. Usui, and C. Parimi. Arbitrary discontinuities in finite elements. *International Journal for Numerical Methods in Engineering*, 50:993–1013, 2001.

[5] Nicolas Moës and Ted Belytschko. Extended finite element method for cohesive crack growth. *Engineering fracture mechanics*, 69:813–833, 2002.

[6] Viggo Tvergaard. Cohesive zone representation of failure between elastic or rigid solids and ductile solids. *Engineering Fracture Mechanics*, 70:1859–1868, 2003.

[7] H Samet. *The design and analysis of spatial data structures*. Reading, Mass. [u.a.] : Addison-Wesley, 1994.

[8] N. Sukumar. Construction of polygonal interpolants: a maximum entropy approach. *International Journal for Numerical Methods in Engineering*, 61:2159–2181, 2004.

[9] T.K. Hellen. On the method of virtual crack extension. *International journal for numerical methods in engineering*, 9(1):187–207, 1975.

[10] B. Winkler. *Traglastuntersuchungen von unbewehrten und bewehrten Betonstrukturen auf der Grundlage eines objektiven Werkstoffgesetzes für Beton*. PhD thesis, University of Innsbruck, 2001.

[11] M.B. Nooru-Mohamed. *Mixed-mode fracture of concrete: An experimental approach*. PhD thesis, Delft University of Technology, Delft, 1992.

[12] Christian Feist, Walter Kerber, Hermann Lehar, and Günter Hofstetter. A comparative study of numerical models for concrete cracking. In P. Neittaanmäki, T. Rossi, Korotov S., E. Oñate, J. Périaux, and D. Knörzer, editors, *Proceedings of the European Congress on Computational Methods in Applied Sciences and Engineering, ECCOMAS*, 2004.